FAME: Adaptive Functional Attention with Expert Routing for Function-on-Function Regression

Yifei Gao
Department of Industrial Engineering
Tsinghua University
Beijing 100084, China
gao-yf@mail.tsinghua.edu.cn

Yong Chen
Department of Industrial and Systems Engineering
University of Iowa
Iowa City, IA 52242, USA
yong-chen@uiowa.edu

Chen Zhang[*]
Department of Industrial Engineering
Tsinghua University
Beijing 100084, China
zhangchen01@tsinghua.edu.cn

Abstract

Functional data play a pivotal role across science and engineering, yet their infinite-dimensional nature makes representation learning challenging. Conventional statistical models depend on pre-chosen basis expansions or kernels, limiting the flexibility of data-driven discovery, while many deep-learning pipelines treat functions as fixed-grid vectors, ignoring inherent continuity. In this paper, we introduce **F**unctional **A**ttention with a **M**ixture-of-**E**xperts (FAME), an end-to-end, fully data-driven framework for function-on-function regression. FAME forms continuous attention by coupling a bidirectional neural controlled differential equation with MoE-driven vector fields to capture intra-functional continuity, and further fuses change to inter-functional dependencies via multi-head cross attention. Extensive experiments on synthetic and real-world functional regression benchmarks show that FAME achieves state-of-the-art accuracy and strong robustness to arbitrarily sampled discrete observations of functions.

1 Introduction

Functional data are samples whose individual elements are random continuous functions, providing rich temporal–spatial dynamics in domains such as biology [13], marketing [11], transportation [17], and meteorology [42]. With the growing demand for high-resolution measurements, functional data analysis (FDA) is attracting increasing attention in both scientific research and practical applications [41, 27, 20, 48]. Among canonical problems in functional data analysis (FDA), **function-on-function regression (FoFR)** is widely regarded as the most challenging and representative task, as it requires the model to accommodate both infinite-dimensional inputs and outputs. [35, 25, 9]. While functional data offer new opportunities, they also bring intertwined challenges: **(1) Intra-functional continuity**: each function lies in infinite-dimensional continuous functional space with features such as local dynamics and global trends [29]; **(2) Inter-functional interactions**: different dimensions of the input function can have nonlinear couplings with each other [6]; **(3) Feature heterogeneity**: different functions may exhibit vastly different properties such as scale, smoothness, or noise, and may even reside in different functional spaces [7].

[*] Corresponding author

39th Conference on Neural Information Processing Systems (NeurIPS 2025).

To address these challenges, existing approaches broadly fall into two methodological categories. The first category comprises classical statistical methods, which manage functional complexity by projecting each function onto finite-dimensional representations. Common techniques include basis expansions, such as B-splines [5], wavelets [49], and functional principal component analysis (FPCA) [8], as well as kernel-based methods that embed functions into functional reproducing kernel Hilbert spaces via operator-valued kernels [4]. Although these methods facilitate linear or additive modeling in lower-dimensional spaces, their performance heavily depends on predefined bases or kernels and strong smoothness assumptions, limiting their ability to capture intra-functional and inter-functional features prevalent in real-world functional data. The second category involves recent deep learning approaches, which offer greater flexibility inspired by advances in natural language processing and computer vision. These methods typically feed discretized curves into deep neural networks. For instance, Shi et al. [33] proposes a smooth-kernel neural network tailored to nonlinear functional regression. Yao et al. [45] introduces adaptive basis learners that adjust expansions according to specific tasks. Although such models enhance nonlinearity and support end-to-end learning, they still assume all functions lie in discretized regular sampling grids with the same dimension, and treat functional data as finite-dimensional vectors. Consequently, these methods have limited power to model intra-functional continuous dynamics, and cannot be applied to irregularly sampled cases, let alone handle feature heterogeneity.

To overcome these limitations, we introduce Functional Attention with Mixture-of-Experts (FAME), an end-to-end framework designed expressly for FOFR. Specifically, our contributions are: (1) FAME is the first FoFR model that directly operates on irregularly sampled functional space without relying on predefined basis functions or discretisation grids. Its effectiveness is rigorously established through both theoretical guarantees and extensive experimental validation. (2) FAME includes a novel functional attention mechanism composed of continuous attention via bidirectional Neural controlled differential equations (NCDEs), which can efficiently capture intra-functional continuity, and multi-head cross attention, which can efficiently model inter-functional interactions. (3) FAME enhances a mixture-of-experts (MoE) architecture, enabling adaptive modeling of feature heterogeneity, and incorporates an NCDE decoder capable of generating continuous functional outputs at arbitrary query locations, naturally accommodating misaligned target indices.

2 Related work

Function-on-function regression FoFR has witnessed substantial advances in recent years and is drawing increasing attention from the research community. Existing approaches can be concretely divided into three categories: linear decomposition, reproducing kernel Hilbert space (RKHS), and deep learning methods. Linear approaches employ finite bases such as FPCA, wavelets, or splines to project input and response curves into low-dimensional coordinates, enabling conventional regression techniques [44, 24, 23, 22, 28]. Despite computational efficiency, these approaches rely on fixed bases, restricting their ability to capture non-stationary dynamics and complex interactions. RKHS-based methods use operator-valued kernels, providing nonlinear function regression within linear frameworks [19, 14]. Extensions have incorporated robust losses [16] and optimal estimation strategies [35], yet kernel selection and scalability remain persistent challenges. Deep learning methods, including functional neural networks (FNNs) [30], FPCA-based neural networks [39, 40], and adaptive basis expansions [45], offer data-driven flexibility. However, these techniques typically discretize functions onto fixed grids, ignoring the inherent continuity and heterogeneity of functional data. In summary, current methods rely on either predefined or prematurely discretized feature representation for functional data, limiting their ability to model complex FoFR problems comprehensively.

Neural differential equations Neural differential equations provide a powerful framework that combines continuous-time dynamics with the high-capacity function approximation of neural networks, making them particularly effective for handling irregular time series [31, 12]. Among these methods, Neural ODEs map discrete data to continuous trajectories and leverage adjoint methods for memory-efficient gradient computation, enabling scalable training for large models [1]. Building on this concept, Neural CDEs [15] extend the approach by capturing the continuous-time dynamics of RNNs through a learned control function for hidden states. This strategy has shown superior performance in modeling irregular time series compared to Neural ODEs or RNNs, particularly in offline prediction tasks [3]. Recent work also emphasizes their usefulness in enhancing stability and generalization by injecting noise directly into the training process [26]. However, Neural CDEs operate in a strictly causal fashion, building hidden-state dynamics solely from past observations, whereas FoFR can exploit the full input function to capture global dependencies and non-causal relationships.

Attention mechanism for feature representation The attention mechanism was initially proposed to mitigate the limitations of encoding sequences into fixed-length vectors in RNN-based models [2]. Xu et al. [43] introduces soft alignment during decoding, enabling better handling of long sequences. This concept evolves through variants like global and local attention, and reaches a milestone with the Transformer architecture [37], which entirely replaces recurrence with self-attention, improving both modeling power and computational efficiency. Building on this foundation, numerous attention-based models have emerged for time series modeling. For example, iTransformer[21] reorganises the input so that time steps serve as channels and variables act as tokens, allowing self-attention to capture long-range temporal dependencies more effectively, whereas CrossFormer[47] employs a frequency-aware, cross-scale attention mechanism to model long- and short-term patterns simultaneously. However, these attention mechanisms are designed for discrete sequences defined on fixed grids. They do not provide a native framework for continuous-space mapping of functions.

3 Function-on-function regression

We consider an unknown operator $\mathcal{T} : \mathcal{X} \to \mathcal{Y}$ that maps a d-tuple of input functions $X = (X^{(1)}, \dots, X^{(d)})$ to an m-tuple of output functions $Y = (Y^{(1)}, \dots, Y^{(m)})$. For every input channel $j \in \{1, \dots, d\}$ the function $X^{(j)} : [0, T_j] \to \mathbb{R}$ is assumed to have finite 1-variation; we denote the space by

$$\mathcal{V}_j = \big\{ X^{(j)} : [0, T_j] \to \mathbb{R} \mid \|X^{(j)}\|_{1-\mathrm{var}} < \infty \big\}, \quad \mathcal{X} = \mathcal{V}_1 \times \cdots \times \mathcal{V}_d.$$

For each output index $\zeta \in \{1, \dots, m\}$, the output function $Y^{(\zeta)} : [0, S_\zeta] \to \mathbb{R}$ is continuous and equipped with the supremum norm $\|Y^{(\zeta)}\|_\infty = \sup_{s \in [0, S_\zeta]} |Y^{(\zeta)}(s)|$. We set

$$\mathcal{W}_\zeta = C\big([0, S_\zeta], \mathbb{R}\big), \quad \mathcal{Y} = \mathcal{W}_1 \times \cdots \times \mathcal{W}_m, \quad \|Y\|_\infty = \max_\zeta \|Y^{(\zeta)}\|_\infty.$$

In practice, for each sample i we observe $X_i = (X_i^{(1)}, \dots, X_i^{(d)}) \in \mathcal{X}, \quad Y_i = (Y_i^{(1)}, \dots, Y_i^{(m)}) \in \mathcal{Y}$, but only at irregular time points $\{(t_{i,\ell}, x_{i,\ell})\}_{\ell=1}^{\Lambda_i}$ for each $X_i^{(j)}$ and $\{(s_{i,r}, y_{i,r})\}_{r=1}^{\Gamma_i}$ for each $Y_i^{(\zeta)}$. Given a dataset $\{(X_i, Y_i)\}_{i=1}^{N_s} \subset \mathcal{X} \times \mathcal{Y}$, our goal is to learn a finite-parameter approximation $\mathcal{T}_\theta$ that recovers $\mathcal{T}$ from these discretely and non-uniformly observed functions.

4 Functional attention with a mixture-of-experts (FAME)

In this section, we describe how FAME addresses the core challenges of FoFR by designing a custom functional attention mechanism. Figure 1 presents a high-level overview of the overall architecture of FAME. To account for the truly infinite-dimensional nature of each function $X^{(j)}$, we introduce in Section 4.1 a continuous attention block built on a bidirectional NCDE that integrates both forward and backward over t. This construction produces smoothly varying Query, Key, and Value trajectories, ensuring that every query instant attends to both past and future contexts and remains insensitive to the discrete sampling along the input function. To capture heterogeneity across functions, Section 4.2 enhances this continuous attention block by replacing its single vector field with a mixture of K expert fields (MoE), each specialised for distinct scales, amplitudes, or noise regimes. A learnable router allocates a weight vector over the K experts, thereby boosting the model's ability to capture feature heterogeneity, removing the need to instantiate a separate encoder for each function, and enabling smooth generalisation to unseen features. Section 4.3 then introduces a cross attention fusion block that integrates these per-function representations into a unified global context, propagating information across functions and modelling their continuously evolving, nonlinear couplings, before decoding via a NCDE head to produce the final continuous output.

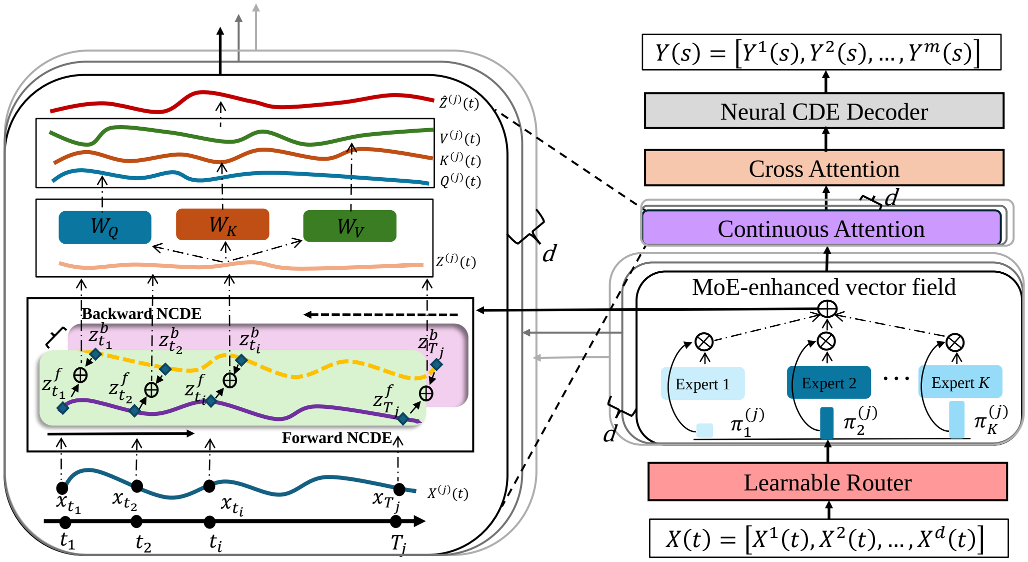

Figure 1: Architecture of the FAME.

4.1 Capturing intra-functional continuity through continuous attention

Controlled differential equations. The core motivation of our method is to construct attention mechanisms that operate directly on continuous functional data. We adopt the framework of neural controlled differential equations (NCDEs), whose integrals are interpreted in the Young sense because every input function has finite 1-variation. In a controlled differential equation (CDE)[15], an external driver continuously influences the internal dynamics, providing a principled route for learning from irregularly sampled paths. Formally, the latent trajectory is defined as the solution of:

$$z(t) = z(t_0) + \int_{t_0}^{t} f_\theta\big(z(u)\big)\, dX(u), \qquad t \in (t_0, T_j], \tag{1}$$

where the initial state $z(t_0) = \xi_\theta\big(X(t_0), t_0\big)$ is learnable, $z(t)$ encodes an evolving summary of the input path, and f_θ governs how this summary changes in response to the signal X.

Bidirectional NCDE. A one-sided CDE only observes the driving signal on $[t_0, t]$, so its latent state lacks access to the future segment $(t, T_j]$. To capture the essential global structure of functional data, we propose a bidirectional NCDE that augments the standard forward integration with a complementary backward pass. For each function $X^{(j)}$, we solve a pair of controlled differential equations:

$$\begin{aligned} Z_{\text{fwd}}^{(j)}(t) &= Z^{(j)}(t_0) + \int_{t_0}^{t} f_{\theta_j^{\text{fwd}}}\big(Z_{\text{fwd}}^{(j)}(\tau)\big)\, dX^{(j)}(\tau), \\ Z_{\text{bwd}}^{(j)}(t) &= Z^{(j)}(T_j) - \int_{t}^{T_j} f_{\theta_j^{\text{bwd}}}\big(Z_{\text{bwd}}^{(j)}(\tau)\big)\, d\tilde{X}^{(j)}(\tau), \end{aligned} \qquad t \in [t_0, T_j], \tag{2}$$

where $f_{\theta_j^{\text{fwd}}}$ and $f_{\theta_j^{\text{bwd}}}$ are direction-specific vector fields, and $\tilde{X}^{(j)}$ denotes the reversed input function $\tilde{X}^{(j)}(t) = X^{(j)}(T_j - t)$.

Assumption 1 (Directional Lipschitz regularity)**.** *Each vector field is globally Lipschitz: that is, $f_{\theta_j^{fwd}}$ is L_j^{fwd}-Lipschitz and $f_{\theta_j^{bwd}}$ is L_j^{bwd}-Lipschitz.*

Theorem 1 (Existence and uniqueness of the Bi-NCDE)**.** *Under Assumption 1, both the forward and backward CDEs in* (2) *admit unique solutions on $[t_0, T_j]$. Moreover, letting $L_j = \max\{L_j^{fwd}, L_j^{bwd}\}$, the latent paths satisfy*

$$\big\|Z^{(j)} - \tilde{Z}^{(j)}\big\|_\infty \;\le\; e^{L_j(T_j - t_0)}\, \big\|X^{(j)} - \tilde{X}^{(j)}\big\|_{1\text{-}var}.$$

Then, the final latent representation is defined as $Z^{(j)}(t) = [Z^{(j)}_{\text{fwd}}(t),\, Z^{(j)}_{\text{bwd}}(t)] \in \mathbb{R}^{2h}$, combining local dynamics with global context.

Continuous attention. To extend attention from discrete sequences to continuous functions, we apply three bounded matrices $W_Q,\, W_K,\, W_V \in \mathbb{R}^{d_f \times 2h}$ to $Z^{(j)}(t)$, thereby obtaining continuous Query, Key, and Value functions:

$$Q^{(j)}(t) = W_Q\, Z^{(j)}(t), \quad K^{(j)}(t) = W_K\, Z^{(j)}(t), \quad V^{(j)}(t) = W_V\, Z^{(j)}(t), \quad t \in [t_0, T_j]. \tag{3}$$

Because bounded linear maps preserve Young-integrability and Lipschitz regularity, the ensuing attention operations are well defined over $[t_0, T_j]$ and reserve the continuous structure of the data. For any (t, τ), we compute the attention score and normalized weight

$$\alpha^{(j)}(t,\tau) = \frac{\langle Q^{(j)}(t), K^{(j)}(\tau)\rangle}{\sqrt{d_f}}, \qquad \hat{\alpha}^{(j)}(t,\tau) = \frac{e^{\alpha^{(j)}(t,\tau)}}{\displaystyle\int_{t_0}^{T_j} e^{\alpha^{(j)}(t,u)}\, du}, \tag{4}$$

and form the attended representation

$$\hat{Z}^{(j)}(t) = \int_{t_0}^{T_j} \hat{\alpha}^{(j)}(t,\tau)\, V^{(j)}(\tau)\, d\tau, \qquad t \in [t_0, T_j]. \tag{5}$$

Assumption 2 (Normalization regularity)**.** *There exists $\gamma > 0$ such that $\int_{t_0}^{T_j} e^{\alpha^{(j)}(t,s)}\, ds \geq \gamma$ for all t and admissible inputs. In practice we ensure this by a temperature parameter $\tau^{\text{temp}} \geq \tau_0^{\text{temp}} > 0$ and log-sum-exp stabilisation.*

Proposition 1 (Lipschitz stability)**.** *Under Assumptions 1 and 2,*

$$\big\|\hat{Z}^{(j)} - \hat{\tilde{Z}}^{(j)}\big\|_\infty \leq \frac{\|W_V\|}{\gamma}\, e^{L_j(T_j - t_0)} L_j(T_j - t_0)\, \big\|X^{(j)} - \tilde{X}^{(j)}\big\|_{1\text{-}var}.$$

Denote the constant on the right by L_{single} for later reference.

Proposition 2 (Universal approximation)**.** *Let $k \in C([t_0, T_j]^2)$ and $\varepsilon > 0$. If $d_f \geq h$ and the width of f_θ is sufficiently large, then there exist parameters $(f_\theta, W_Q, W_K, W_V)$ with $\big\|\alpha^{(j)} - k\big\|_\infty < \varepsilon$. Hence $X^{(j)} \mapsto \hat{Z}^{(j)}$ can approximate any bounded continuous operator on functions, independent of the sampling grid;*

Proposition 1 confirms the Lipschitz stability of our continuous attention mechanism: a small perturbation of the input function produces only a proportionally small change in its attended representation. Moreover, Proposition 2 shows that, with sufficient width, the continuous attention can approximate any bounded continuous kernel and thus emulate arbitrary integral operators in FoFR. Consequently, by embedding continuous attention within a bidirectional NCDE, our model not only captures both local dynamics and global context but also can realize any mapping in the function space. More details are provided in Appendix A.

4.2 Encoding feature-wise heterogeneity with MoE-Driven Bi-NCDE

Real-world functional data exhibit evident feature heterogeneity, as each function may vary on its own scale, frequency, and noise level. A single vector field can scarcely accommodate such diversity. To address this, we assign each function its own MoE vector field. Specifically, a shared router computes, once per function, a fixed convex combination of K specialist fields, which then governs the bidirectional NCDE dynamics for that function.

Function-wise router and expert fields. Let $\{f_{\theta_k} : \mathbb{R}^h \to \mathbb{R}^h\}_{k=1}^K$ be K expert vector fields. For each input function $X^{(j)}$ we compress its functional information with a lightweight 1-D convolution followed by global average pooling, obtaining a summary vector $s^{(j)} = \operatorname{ConvPool}\big(X^{(j)}\big) \in \mathbb{R}^{h_0}$. The router $g_\phi : \mathbb{R}^{h_0} \to \mathbb{R}^K$ assigns softmax weights $\pi^{(j)} = \operatorname{softmax}\big(g_\phi(s^{(j)})\big) \in \Delta^{K-1}$ to the K specialist fields, yielding the MoE vector field

$$f_\Theta^{(j)}(z) = \sum_{k=1}^{K} \pi_k^{(j)}\, f_{\theta_k}(z), \qquad \Theta = \{\theta_1, \ldots, \theta_K, \phi\}. \tag{6}$$

Directional experts with a shared router. To preserve the bidirectional representation we instantiate disjoint expert sets $\{f_{\theta_k^{\mathrm{fwd}}}\}$ and $\{f_{\theta_k^{\mathrm{bwd}}}\}$, yet reuse the same gates $\pi^{(j)}$ in both directions:

$$f^{(j)}_{\Theta^{\mathrm{fwd}}}(z) = \sum_k \pi_k^{(j)} \, f_{\theta_k^{\mathrm{fwd}}}(z), \qquad f^{(j)}_{\Theta^{\mathrm{bwd}}}(z) = \sum_k \pi_k^{(j)} \, f_{\theta_k^{\mathrm{bwd}}}(z).$$

Assumption 3 (MoE regularity)**.** *Each expert $f_{\theta_k^{fwd}}$ and $f_{\theta_k^{bwd}}$ is globally L_k^{fwd}- and L_k^{bwd}-Lipschitz, respectively, and bounded by B_k^{fwd} and B_k^{bwd}. The router g_ϕ is bounded on the summary space: $\|g_\phi(s)\|_\infty \le B_g$ for all $s \in \mathbb{R}^{h_0}$.*

Lemma 1 (Mixed-field Lipschitz bound)**.** *Under Assumption 3, the mixed fields $f^{(j)}_{\Theta^{fwd}}$ and $f^{(j)}_{\Theta^{bwd}}$ are globally Lipschitz with*

$$L_{mix} = \max\Big\{\sum_k \pi_k^{(j)} L_k^{fwd}, \ \sum_k \pi_k^{(j)} L_k^{bwd}\Big\} \ \le \ \max_k\big(L_k^{fwd}, L_k^{bwd}\big).$$

Consequently, the bidirectional NCDE driven by (6) *satisfies the existence, uniqueness, and stability properties of Theorem 1.*

MoE-Driven Bi-NCDE. Replacing $f_{\theta_j^{\mathrm{fwd}}}$ and $f_{\theta_j^{\mathrm{bwd}}}$ in (2) with $f^{(j)}_{\Theta^{\mathrm{fwd}}}$ and $f^{(j)}_{\Theta^{\mathrm{bwd}}}$ yields the MoE-Driven Bi-NCDE, which enables each input function to employ a custom vector field mixture and thereby model input functions with markedly different characteristics.

Theorem 2 (Well-posed MoE-Driven Bi-NCDE)**.** *The MoE augmentation admits unique solutions, and the stability bound* (1) *holds with $L_j = \max\{L^{fwd}_{mix}, L^{bwd}_{mix}\}$.*

Thus the MoE design endows the encoder with function-wise expressiveness while retaining all continuity, sampling invariance, and Lipschitz stability guarantees of the base architecture.

4.3 Integrating inter-functional interactions via cross attention

Having obtained a function-wise representation $\hat{Z}^{(j)}$ for each input function, we now capture the inter-functional dependencies that single-channel encoders miss. We realise this with a multi-head cross attention that, at every time point t, allows each function to attend to the concurrent states of all other functions.

Cross attention. For every head $p \in \{1, \dots, M\}$ and function $j \in \{1, \dots, d\}$, shared linear maps $W_Q^{(p)}, W_K^{(p)}, W_V^{(p)} \in \mathbb{R}^{d_c \times d_f}$ project the latent paths into query, key, and value functions:

$$Q^{(j,p)}(t) = W_Q^{(p)} \hat{Z}^{(j)}(t), \quad K^{(j,p)}(t) = W_K^{(p)} \hat{Z}^{(j)}(t), \quad V^{(j,p)}(t) = W_V^{(p)} \hat{Z}^{(j)}(t). \tag{7}$$

Cross attention weights are defined by

$$\hat{\beta}^{(j,\ell,p)}(t) = \frac{\exp\{\langle Q^{(j,p)}(t), K^{(\ell,p)}(t)\rangle / \sqrt{d_c}\}}{\displaystyle\sum_{r=1}^{d} \exp\{\langle Q^{(j,p)}(t), K^{(r,p)}(t)\rangle / \sqrt{d_c}\}}, \qquad \ell \in \{1, \dots, d\}. \tag{8}$$

and each head outputs

$$H^{(j,p)}(t) = \sum_{\ell=1}^{d} \hat{\beta}^{(j,\ell,p)}(t) \, V^{(\ell,p)}(t). \tag{9}$$

Concatenating the M heads and applying $W_O \in \mathbb{R}^{2h \times M d_c}$ gives

$$H^{(j)}(t) = W_O \big[H^{(j,1)}(t) \| \dots \| H^{(j,M)}(t)\big], \qquad t \in [t_0, T_j]. \tag{10}$$

Here W_O projects the concatenated representation back to the original $2h$-dimensional latent space, keeping the hidden width uniform throughout the network.

Assumption 4 (Cross attention Lipschitz)**.** *For every head $p \in \{1, \dots, M\}$ the projection matrices satisfy $\|W_Q^{(p)}\|_{\mathrm{op}}, \|W_K^{(p)}\|_{\mathrm{op}}, \|W_V^{(p)}\|_{\mathrm{op}}, \|W_O\|_{\mathrm{op}} \le M_{mat}$ for some constant $M_{mat} > 0$. Under this condition, the cross attention map $\hat{Z} \mapsto H$ is globally L_{cross}-Lipschitz with $L_{cross} \le (M_{mat})^2 / \sqrt{d_c}$ with respect to the* 1*-variation norm on function space; see Appendix A.1 for the derivation.*

CDE decoder for functional targets. To produce continuous functional outputs, we feed the stacked path $H(t) = \big[H^{(1)}(t)\| \dots \|H^{(d)}(t)\big] \in \mathbb{R}^{2hd}$ into a shallow neural CDE:

$$\hat{Y}^{(\zeta)}(s) = y^{(\zeta)}(s_0) + \int_0^s f_\psi\big(\hat{Y}^{(\zeta)}(u)\big)\, dH(u), \qquad s \in [0, S_\zeta], \tag{11}$$

where $f_\psi : \mathbb{R}^m \to \mathbb{R}^m$ is a learnable vector field. Because the solution of (11) can be evaluated at *any* index s, the decoder naturally accommodates misaligned or irregular target grids.

Assumption 5 (Decoder Lipschitz regularity)**.** *The decoder field f_ψ is globally L_ψ-Lipschitz and bounded: $\|f_\psi\|_\infty \le B_\psi$.*

Theorem 3 (Well-Posedness and Lipschitz stability of the decoder)**.** *Under Assumptions 4–5, the encoder output path H has finite 1-variation, and (11) admits a unique solution $\hat{Y}^{(\zeta)} \in C\big([0, S_\zeta], \mathbb{R}\big)$ with*

$$\|\hat{Y}^{(\zeta)} - \tilde{Y}^{(\zeta)}\|_\infty \le e^{L_\psi S_\zeta} L_\psi S_\zeta \, \|H - \tilde{H}\|_{1\text{-}var}.$$

Hence, for each output index ζ, the decoder $\mathcal{D}_\psi : H \mapsto \hat{Y}^{(\zeta)}$ is a bounded, continuous operator from $\big(C([0, S_\zeta], \mathbb{R}^{2hd}), \|\cdot\|_{\text{1-var}}\big)$ to the Banach space $\big(C([0, S_\zeta], \mathbb{R}), \|\cdot\|_\infty\big)$.

End-to-end Lipschitz bound and generalization. Composing the encoder $\mathcal{E}_\theta : X \mapsto H$ (continuous and cross attention) with the decoder $\mathcal{D}_\psi : H \mapsto \hat{Y}$ yields the operator $\mathcal{T}_\Theta = \mathcal{D}_\psi \circ \mathcal{E}_\theta$. Denote $S_{\max} = \max_\zeta S_\zeta$. Under the preceding assumptions, $\mathcal{T}_\Theta$ is globally Lipschitz with

$$L_* = L_{\text{enc}}\, e^{L_\psi S_{\max}} L_\psi S_{\max}, \qquad L_{\text{enc}} = L_{\text{cross}}\, L_{\text{single}}.$$

This single constant summarizes the theory behind FAME: the model is provably stable, invariant to sampling grids, and enough to represent any continuous operator on functions. Moreover, the hypothesis class has Rademacher complexity $\mathcal{O}\big(L_*/\sqrt{N}\big)$, supplying a quantitative generalization guarantee for FoFR. Further details and auxiliary lemmas are provided in Appendix A.

5 Experiments

To evaluate the proposed model, we benchmark FAME against a wide range of state-of-the-art methods for FoFR (see Section 2). For basis–expansion pipelines [38], we pair two orthonormal systems—B-splines and Fourier functions—with four classical regressors: Ordinary Linear, Ridge, Lasso, and Elastic Net. Beyond these eight variants, we include functional principal component analysis (FPCA) [8], operator-valued kernel regression [14], Gaussian processes [32], and the functional neural network (FNN) [36] as stronger baselines. We evaluate FAME and the baselines on both synthetic datasets and several real-world datasets, using mean-squared error (MSE) as the primary evaluation metric.

5.1 Datasets

Synthetic data. We generate functional data using Gaussian-process trajectories because GP paths have finite 1-variation almost surely, hence $X_i \in \mathcal{X}$. Specifically, we draw $X_i^{(j)}(t) \sim \mathcal{GP}\big(0, K(t,t')\big)$ for $j = 1, \dots, d$ and $t \in [0,1]$, and define the response by $Y_i(t) = \sin\!\big(\sum_{j=1}^d X_i^{(j)}(t)\big) + \lambda\, \varepsilon_i(t)$, with $\varepsilon_i(t) \overset{\text{i.i.d.}}{\sim} \mathcal{N}(0, \sigma^2)$ and noise level $\lambda \ge 0$. Input and output are sampled on (possibly distinct) irregular grids $\{t_{i,\ell}\}_{\ell=1}^{\Lambda_i}$ and $\{s_{i,r}\}_{r=1}^{\Gamma_i}$. We set $d = 3,\ m = 1,\ \Lambda_i = \Gamma_i = 20$ and $N_s = 200$ unless otherwise specified. In particular, we evaluate FAME under seven controlled settings. **Case 1** fixes the input and output grids at $\Lambda_i = \Gamma_i = 20$, perfectly aligned across all samples. **Case 2** increases the shared resolution to $\Lambda_i = \Gamma_i = 50$, while preserving grid alignment. **Case 3** keeps the output grid at $\Gamma_i = 20$ but samples the input resolution independently as $\Lambda_i \in \{10, 20, 50\}$ for each sample, thereby introducing variable input granularity. Throughout Cases 1–3 we vary the dataset size $N_s \in \{100, 200, 500\}$ to disentangle the effects of resolution and sample size. Moving to stress tests, **Case 4** introduces feature heterogeneity by assigning each input function a distinct RBF kernel width $\sigma_j \in \{0.2, 0.3, 0.5\}$, rather than the fixed value of 0.3 used in the other cases. **Case 5** probes noise robustness by adding independent Gaussian perturbations of noise level $\lambda \in \{0.1, 0.2, 0.3\}$ to every output. **Case 6** tests multivariate prediction by extending the target

Table 1: Average test MSE for different methods in regression. Detailed results (mean ± standard deviation) are provided in Appendix B. The best MSE for each case is highlighted in bold.

Model		Case 1			Case 2			Case 3		
		100	200	500	100	200	500	100	200	500
B-spline	Linear	0.4720	0.3947	0.3123	0.4135	0.3412	0.2822	0.4958	0.4002	0.3260
	Ridge	0.4264	0.3893	0.3117	0.3960	0.3393	0.2817	0.3869	0.3740	0.3222
	Lasso	0.4098	0.3830	0.3052	0.3856	0.3351	0.2766	0.4132	0.3584	0.3188
	Elastic Net	0.4510	0.3650	0.2874	0.3725	0.3152	0.2583	0.3986	0.3618	0.3190
Fourier	Linear	0.5002	0.4092	0.3224	0.4923	0.3636	0.2896	0.4762	0.3921	0.3547
	Ridge	0.4255	0.3780	0.3149	0.3616	0.3343	0.2841	0.3755	0.3568	0.3328
	Lasso	0.3550	0.3493	0.3135	0.3361	0.3280	0.3001	0.3808	0.3560	0.3247
	Elastic Net	0.3540	0.3325	0.2914	0.3167	0.3070	0.2720	0.3737	0.3496	0.3366
FPCA		0.3717	0.3554	0.3200	0.2890	0.2733	0.2624	0.3812	0.3563	0.3295
Kernel Method		0.2441	0.1728	0.1058	0.1741	0.0923	0.0700	0.2654	0.2445	0.1485
Gaussian Process		0.3405	0.2941	0.2036	0.3905	0.3917	0.2588	0.3031	0.2926	0.3945
FNN		0.3123	0.2083	0.1013	0.1941	0.1142	0.0811	0.3678	0.3571	0.1366
FAME w/o Bi-dir		0.1832	0.0812	0.0654	0.1530	0.0528	0.0355	0.1919	0.0813	0.0368
FAME w/o MoE		0.1870	0.0828	0.0663	0.1578	0.0538	0.0362	0.1972	0.0856	0.0374
FAME w/o Cross-attn		0.1902	0.0815	0.0668	0.1602	0.0544	0.0375	0.1997	0.0879	0.0381
FAME		**0.1806**	**0.0783**	**0.0635**	**0.1532**	**0.0511**	**0.0342**	**0.1954**	**0.0796**	**0.0352**

Table 2: Average test set MSE in regression under simulation. Basis Expansion (best) shows the best result among the 8 basis expansion methods presented in Table 1.

Model	case 4	case 5			case 6	case 7		case 8
		0.1	0.2	0.3		5	10	
Basis Expansion(best)	0.3610	0.3665	0.3944	0.4419	0.3669	0.4501	0.4705	0.5204
FPCA	0.3802	0.3879	0.3956	0.4570	0.3844	0.5284	0.5573	0.5737
Kernel Method	0.1928	0.1440	0.1919	0.2435	0.2022	0.4659	0.5236	0.5895
Gaussian Process	0.2302	0.3079	0.3356	0.3830	0.3434	0.4120	0.4498	0.4762
FNN	0.2102	0.1879	0.2250	0.3438	0.1744	0.4801	0.5164	0.5384
FAME	**0.0798**	**0.0846**	**0.1076**	**0.1420**	**0.0824**	**0.2285**	**0.3330**	**0.3530**

to the two-dimensional map $[\sin(\sum_j X_i^{(j)}(t)),\ \cos(\sum_j X_i^{(j)}(t))]^\top$. **Case 7** stresses scalability by increasing the number of input functions to $d \in \{5, 10\}$ while keeping all other settings unchanged. Finally, to isolate the impact of the hyperparameter K under high dimensionality and heterogeneity, **Case 8** fixes the number of input functions at $d = 10$, generates inputs with RBF kernels of widths $\sigma_j \in \{0.2, 0.3, 0.5\}$, and varies $K \in \{1, 2, 3, 5, 8\}$.

Real-world data. We evaluate the same set of models on three public datasets: 1) *Hawaii Ocean*, which contains five hydrographic depth profiles—temperature, salinity, oxygen, chloropigment, and density—among which different variables are treated as regression targets in turn, with the remaining serving as input functions; 2) *Human3.6M*, a human motion capture dataset consisting of 3-D joint trajectories, where we define three action-specific regression tasks (Walking, Eating, and Sitting); and 3) *ETT-small*, a monthly electricity-transformer dataset used to forecast oil temperature from transformer load curves. Full preprocessing details and task definitions are provided in Appendix B.

5.2 Experimental Results

Table 1 summarizes the performance of FAME and various baselines on the synthetic datasets, clearly demonstrating that FAME consistently achieves the lowest test-set MSE. Other methods based on fixed basis expansions, FPCA, Gaussian processes, or neural networks achieve inferior performance,

Table 3: Average test set MSE in regression on different real-world datasets.

Model	Hawaii ocean		Human3.6M			ETDataset
	Salinity	Temp	Walking	Eating	Sitting down	Oil Temp
Basis Expansion(best)	0.0780	0.0014	0.0359	0.04841	0.0122	0.0365
FPCA	0.0865	0.0025	0.0373	0.0099	0.0121	0.0355
Kernel Method	0.0754	0.0025	0.0373	0.0099	0.0121	0.0355
Gaussian Process	0.0931	0.0022	0.0360	0.0075	0.0107	0.0380
FNN	0.0766	0.0020	0.0373	0.0099	0.0121	0.0355
FAME w/o Bi-dir	0.0751	0.0012	0.0327	0.0035	0.0071	0.0264
FAME w/o MoE	0.0759	0.0013	0.0332	0.0038	0.0075	0.0271
FAME w/o Cross-attn	0.0773	0.0014	0.0344	0.0044	0.0083	0.0286
FAME	**0.0748**	**0.0012**	**0.0325**	**0.0034**	**0.0070**	**0.0262**

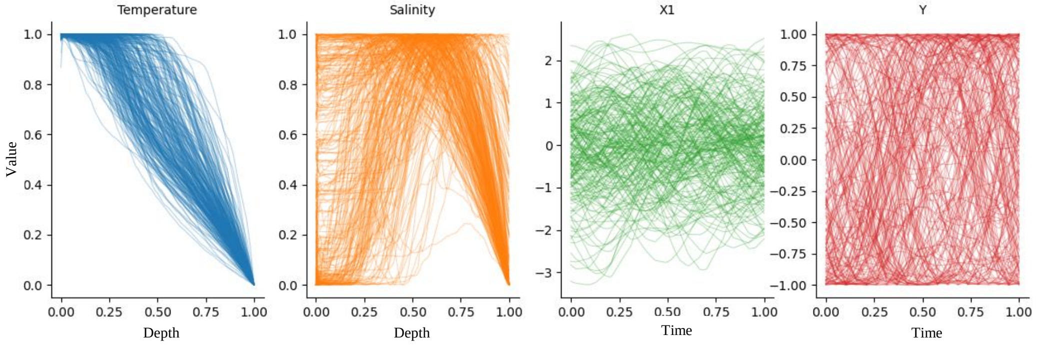

(a) Real data functional features (b) Synthetic data functional features

Figure 2: Visualization of Functional Features.

largely due to their limited capacity to adapt to nonlinear functional mappings, sensitivity to irregular sampling points, or challenges in preserving continuous functional structures. In contrast, FAME's continuous attention mechanism, supported by adaptive MoE-driven dynamics and inter-dimensional cross attention, provides a stable and expressive mapping that directly operates in continuous function spaces, which the ablation study in Table 1 clearly demonstrates. Table 2 further evaluates model robustness across a variety of stress-test scenarios—including feature heterogeneity, noise levels, output structures, and input dimensionalities—demonstrating that FAME consistently maintains superior predictive performance under challenging conditions. Table 3 reports results on real-world datasets, confirming the practical applicability of our model. The performance advantage over strong baselines is reduced compared to the synthetic setting. Figure 2(a) shows that the HAWAII OCEAN dataset occupies a smooth, low-variability subspace dictated by ocean stratification, a structure that fixed-basis and kernel methods can already approximate competently. Figure 2(b) contrasts this with synthetic trajectories drawn from independent Gaussian processes, whose broad, irregular function space contains pronounced local fluctuations. Under this more demanding regime, the continuous-attention encoder in FAME secures a substantially larger accuracy gain, underscoring its flexibility across disparate function-space complexities and corroborating the universal-approximation and sampling-invariance guarantees established in Section 4.3.

As shown in Figure 3, the model's performance varies systematically with key parameters, illustrating clear relationships between predictive behavior and data characteristics. Specifically, in Case 1, the observed test error progressively decreases with increasing sample size (Fig. 3(a)), in agreement with our theoretical generalisation result. Case 2 illustrates a clear improvement in model performance as the number of sampling points grows, with FAME achieving superior accuracy even at a sparse resolution of 10 sampling points (Fig. 3(b)). Case 3 reveals that while baseline methods experience substantial performance degradation under mixed input resolutions, FAME maintains stable and

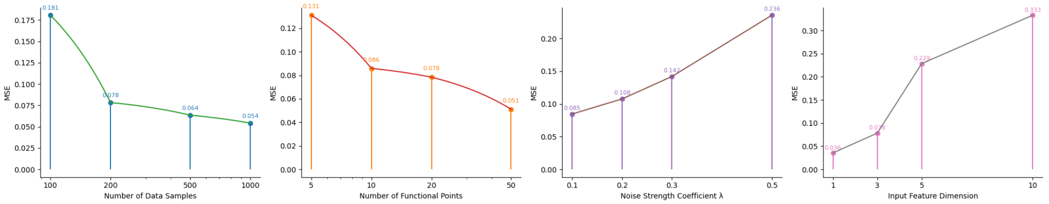

(a) Test MSE by sample size (b) Test MSE by sampling density (c) Test MSE by noise strength (d) Test MSE by input dimensionality

Figure 3: Parameter-sensitivity curves for FAME.

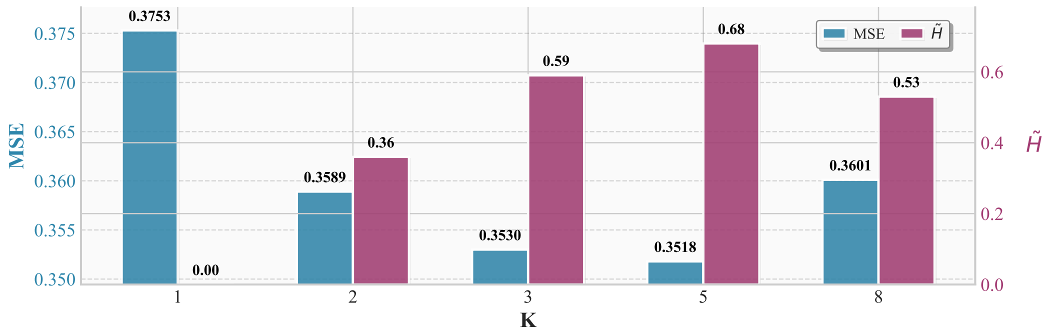

Figure 4: Sensitivity to K—test MSE (left axis) and $\tilde{H}$ (right axis).

superior performance. This result highlights our model's sampling invariance capability, endowed by the Young integral formulation. As the input becomes noisier or more high-dimensional (Cases 4 and 7), all models exhibit increased error (Fig. 3(c),(d)), but FAME remains within a practically useful error range. Taken together, these parameter sweeps confirm that FAME's empirical behaviour matches its theoretical guarantees, maintaining robust accuracy across diverse data regimes. To assess how the number of experts K affects performance, we plot the test MSE together with the normalized routing entropy $\tilde{H} = H/\log K$ in Figure 4, where H denotes the Shannon entropy of the gating distribution and the normalization by $\log K$ yields a $[0, 1]$-scaled quantity comparable across different K. The curves show that accuracy improves as K increases from 1 to 3 and plateaus around $K = 3 \sim 5$, while $\tilde{H}$ remains moderate—indicating healthy, non-collapsed expert utilization. Beyond that, accuracy does not meaningfully improve and computation grows with K. Consequently, $K = 3$ and $K = 5$ show stable accuracy and healthy expert utilization; since computation scales with K, we adopt $K = 3$ as the default. More extensive visualizations and discussions are provided in Appendix B, which also details the experimental setup (hyperparameters, and training schedules) and a comprehensive analysis of computational efficiency (time and memory complexity).

6 Conclusion

We have presented **FAME**, a fully end-to-end framework that learns FoFR mappings by coupling bidirectional neural CDEs with a continuous attention mechanism, enriching the resulting latent dynamics through a mixture-of-experts router, and fusing inter-functional information via multi-head cross attention before decoding with a NCDE. This design yields a resolution-agnostic, Lipschitz-stable, and universally expressive operator that consistently outperforms classical bases, RKHS models, and recent deep networks on both synthetic and real benchmarks. A natural limitation of FAME is that when the underlying operator varies little across the function domain, simpler linear or low-rank models may offer a more attractive trade-off between statistical and computational complexity. In future work, we plan to extend the same functional attention principle beyond FoFR to tasks such as functional classification and function-on-scalar prediction, where the continuity-aware architecture of FAME is expected to provide similar advantages.

Acknowledgement

Yifei Gao and Chen Zhang would like to acknowledge the support of NSFC Grant 72271138 and Tsinghua–NUS Joint Funding 20243080039.

References

[1] Ardizzone , L., Kruse , J., Wirkert , S., Rahner , D., Pellegrini , E. W., Klessen , R. S., Maier-Hein , L., Rother , C., & Köthe , U. (2018) Analyzing inverse problems with invertible neural networks. *arXiv preprint arXiv:1808.04730*

[2] Bahdanau , D., Cho , K., & Bengio , Y. (2014) Neural machine translation by jointly learning to align and translate. *arXiv preprint arXiv:1409.0473*

[3] Bellot , A. & Van Der Schaar , M. (2021) Policy analysis using synthetic controls in continuous-time. In *International Conference on Machine Learning* pages 759–768. PMLR.

[4] Bouche , D., Clausel , M., Roueff , F., & Buc , F. (2021) Nonlinear functional output regression: A dictionary approach. In *International Conference on Artificial Intelligence and Statistics* pages 235–243. PMLR.

[5] Crambes , C., Kneip , A., & Sarda , P. (2009) Smoothing splines estimators for functional linear regression

[6] Fan , Y., James , G. M., & Radchenko , P. (2015) Functional additive regression

[7] Febrero-Bande , M., González-Manteiga , W., & Oviedo De La Fuente , M. (2019) Variable selection in functional additive regression models. *Computational Statistics* **34**:469–487.

[8] Hall , P. & Horowitz , J. L. (2007) Methodology and convergence rates for functional linear regression

[9] Hullait , H., Leslie , D. S., Pavlidis , N. G., & King , S. (2021) Robust function-on-function regression. *Technometrics* **63**(3):396–409.

[10] Ionescu , C., Papava , D., Olaru , V., & Sminchisescu , C. (2013) Human3. 6m: Large scale datasets and predictive methods for 3d human sensing in natural environments. *IEEE transactions on pattern analysis and machine intelligence* **36**(7):1325–1339.

[11] Jank , W. & Zhang , S. (2011) An automated and data-driven bidding strategy for online auctions. *INFORMS Journal on computing* **23**(2):238–253.

[12] Jia , J. & Benson , A. R. (2019) Neural jump stochastic differential equations. *Advances in Neural Information Processing Systems* **32**.

[13] Jiang , F., Cheng , Q., Yin , G., & Shen , H. (2020) Functional censored quantile regression. *Journal of the American Statistical Association* **115**(530):931–944.

[14] Kadri , H., Duflos , E., Preux , P., Canu , S., Rakotomamonjy , A., & Audiffren , J. (2016) Operator-valued kernels for learning from functional response data. *Journal of Machine Learning Research* **17**(20):1–54.

[15] Kidger , P., Morrill , J., Foster , J., & Lyons , T. (2020) Neural controlled differential equations for irregular time series. *Advances in Neural Information Processing Systems* **33**:6696–6707.

[16] Lambert , A., Bouche , D., Szabo , Z., & Buc , F. (2022) Functional output regression with infimal convolution: Exploring the huber and ε-insensitive losses. In *International Conference on Machine Learning* pages 11844–11867. PMLR.

[17] Lan , T., Li , Z., Li , Z., Bai , L., Li , M., Tsung , F., Ketter , W., Zhao , R., & Zhang , C. (2023) Mm-dag: Multi-task dag learning for multi-modal data-with application for traffic congestion analysis. In *Proceedings of the 29th ACM SIGKDD Conference on Knowledge Discovery and Data Mining* pages 1188–1199.

[18] Ledoux , M. & Talagrand , M. (1991) *Probability in Banach Spaces: Isoperimetry and Processes*. *Probability in Banach Spaces: Isoperimetry and Processes*: Springer.

[19] Lian , H. (2007) Nonlinear functional models for functional responses in reproducing kernel hilbert spaces. *Canadian Journal of Statistics* **35**(4):597–606.

[20] Liu , H., You , J., & Cao , J. (2023.) A dynamic interaction semiparametric function-on-scalar model. *Journal of the American Statistical Association* **118**(541):360–373.

[21] Liu , Y., Hu , T., Zhang , H., Wu , H., Wang , S., Ma , L., & Long , M. (2023.) itransformer: Inverted transformers are effective for time series forecasting. *arXiv preprint arXiv:2310.06625*

[22] Luo , R. & Qi , X. (2017) Function-on-function linear regression by signal compression. *Journal of the American Statistical Association* **112**(518):690–705.

[23] Luo , R., Qi , X., & Wang , Y. (2016) Functional wavelet regression for linear function-on-function models

[24] Müller , H.-G. & Yao , F. (2008) Functional additive models. *Journal of the American Statistical Association* **103**(484):1534–1544.

[25] Mutis , M., Beyaztas , U., Karaman , F., & Lin Shang , H. (2025) On function-on-function linear quantile regression. *Journal of Applied Statistics* **52**(4):814–840.

[26] Oh , Y., Lim , D., & Kim , S. (2024) Stable neural stochastic differential equations in analyzing irregular time series data. *arXiv preprint arXiv:2402.14989*

[27] Park , J., Ahn , J., & Jeon , Y. (2022) Sparse functional linear discriminant analysis. *Biometrika* **109**(1): 209–226.

[28] Qi , X. & Luo , R. (2019) Nonlinear function-on-function additive model with multiple predictor curves. *Statistica Sinica* **29**(2):719–739.

[29] Ramsay , J. & Silverman , B. (2007) *Applied Functional Data Analysis: Methods and Case Studies*. *Applied Functional Data Analysis: Methods and Case Studies*: Springer.

[30] Rossi , F. & Conan-Guez , B. (2006) Theoretical properties of projection based multilayer perceptrons with functional inputs. *Neural Processing Letters* **23**(1):55–70.

[31] Rubanova , Y., Chen , R. T., & Duvenaud , D. K. (2019) Latent ordinary differential equations for irregularly-sampled time series. *Advances in neural information processing systems* **32**.

[32] Shi , J. Q. & Choi , T. (2011) *Gaussian process regression analysis for functional data*. *Gaussian process regression analysis for functional data*: CRC press.

[33] Shi , Z., Fan , J., Song , L., Zhou , D.-X., & Suykens , J. A. (2024) Nonlinear functional regression by functional deep neural network with kernel embedding. *arXiv preprint arXiv:2401.02890*

[34] Stone , M. H. (1948) The generalized weierstrass approximation theorem. *Mathematics Magazine* **21**(5): 237–254.

[35] Sun , X., Du , P., Wang , X., & Ma , P. (2018) Optimal penalized function-on-function regression under a reproducing kernel hilbert space framework. *Journal of the American Statistical Association* **113**(524): 1601–1611.

[36] Thind , B., Multani , K., & Cao , J. (2023) Deep learning with functional inputs. *Journal of Computational and Graphical Statistics* **32**(1):171–180.

[37] Vaswani , A., Shazeer , N., Parmar , N., Uszkoreit , J., Jones , L., Gomez , A. N., Kaiser , Ł., & Polosukhin , I. (2017) Attention is all you need. *Advances in neural information processing systems* **30**.

[38] Wang , J.-L., Chiou , J.-M., & Müller , H.-G. (2016) Functional data analysis. *Annual Review of Statistics and its application* **3**(1):257–295.

[39] Wang , Q., Zheng , S., Farahat , A., Serita , S., Saeki , T., & Gupta , C. (2019) Multilayer perceptron for sparse functional data. In *2019 International joint conference on neural networks (IJCNN)* pages 1–10. IEEE.

[40] Wang , Q., Wang , H., Gupta , C., Rao , A. R., & Khorasgani , H. (2020) A non-linear function-on-function model for regression with time series data. In *2020 IEEE International Conference on Big Data (Big Data)* pages 232–239. IEEE.

[41] Wang , S., Cao , G., Shang , Z., & Initiative , A. D. N. (2023) Deep neural network classifier for multidimensional functional data. *Scandinavian Journal of Statistics* **50**(4):1667–1686.

[42] Wen , C., Wang , X., & Zhang , A. (2023) $\ell 0$ trend filtering. *INFORMS Journal on Computing* **35**(6): 1491–1510.

[43] Xu , K., Ba , J., Kiros , R., Cho , K., Courville , A., Salakhudinov , R., Zemel , R., & Bengio , Y. (2015) Show, attend and tell: Neural image caption generation with visual attention. In *International conference on machine learning* pages 2048–2057. PMLR.

[44] Yao , F., Müller , H.-G., & Wang , J.-L. (2005) Functional linear regression analysis for longitudinal data

[45] Yao , J., Mueller , J., & Wang , J.-L. (2021) Deep learning for functional data analysis with adaptive basis layers. In *International Conference on Machine Learning* pages 11898–11908. PMLR.

[46] Young , L. C. (1936) An inequality of the hölder type, connected with stieltjes integration

[47] Zhang , Y. & Yan , J. (2023) Crossformer: Transformer utilizing cross-dimension dependency for multivariate time series forecasting. In *The eleventh international conference on learning representations*

[48] Zhang , Z., Wang , X., Kong , L., & Zhu , H. (2022) High-dimensional spatial quantile function-on-scalar regression. *Journal of the American Statistical Association* **117**(539):1563–1578.

[49] Zhao , Y., Ogden , R. T., & Reiss , P. T. (2012) Wavelet-based lasso in functional linear regression. *Journal of computational and graphical statistics* **21**(3):600–617.

[50] Zhou , H., Zhang , S., Peng , J., Zhang , S., Li , J., Xiong , H., & Zhang , W. (2021) Informer: Beyond efficient transformer for long sequence time-series forecasting. In *The Thirty-Fifth AAAI Conference on Artificial Intelligence, AAAI 2021, Virtual Conference 35*, pp. 11106–11115. AAAI Press.

NeurIPS Paper Checklist

The checklist is designed to encourage best practices for responsible machine learning research, addressing issues of reproducibility, transparency, research ethics, and societal impact. Do not remove the checklist: **The papers not including the checklist will be desk rejected.** The checklist should follow the references and follow the (optional) supplemental material. The checklist does NOT count towards the page limit.

Please read the checklist guidelines carefully for information on how to answer these questions. For each question in the checklist:

- You should answer [Yes] , [No] , or [NA] .
- [NA] means either that the question is Not Applicable for that particular paper or the relevant information is Not Available.
- Please provide a short (1–2 sentence) justification right after your answer (even for NA).

The checklist answers are an integral part of your paper submission. They are visible to the reviewers, area chairs, senior area chairs, and ethics reviewers. You will be asked to also include it (after eventual revisions) with the final version of your paper, and its final version will be published with the paper.

The reviewers of your paper will be asked to use the checklist as one of the factors in their evaluation. While "[Yes] " is generally preferable to "[No] ", it is perfectly acceptable to answer "[No] " provided a proper justification is given (e.g., "error bars are not reported because it would be too computationally expensive" or "we were unable to find the license for the dataset we used"). In general, answering "[No] " or "[NA] " is not grounds for rejection. While the questions are phrased in a binary way, we acknowledge that the true answer is often more nuanced, so please just use your best judgment and write a justification to elaborate. All supporting evidence can appear either in the main paper or the supplemental material, provided in appendix. If you answer [Yes] to a question, in the justification please point to the section(s) where related material for the question can be found.

IMPORTANT, please:

- **Delete this instruction block, but keep the section heading “NeurIPS paper checklist"**,
- **Keep the checklist subsection headings, questions/answers and guidelines below.**
- **Do not modify the questions and only use the provided macros for your answers**.

1. **Claims**

   Question: Do the main claims made in the abstract and introduction accurately reflect the paper’s contributions and scope?

   Answer: **[TODO]**Yes

   Justification: **[TODO]**The abstract and introduction present the proposed model and key innovations, which are fully supported by the methodological and experimental sections.

   Guidelines:

   - The answer NA means that the abstract and introduction do not include the claims made in the paper.
   - The abstract and/or introduction should clearly state the claims made, including the contributions made in the paper and important assumptions and limitations. A No or NA answer to this question will not be perceived well by the reviewers.
   - The claims made should match theoretical and experimental results, and reflect how much the results can be expected to generalize to other settings.
   - It is fine to include aspirational goals as motivation as long as it is clear that these goals are not attained by the paper.

2. **Limitations**

   Question: Does the paper discuss the limitations of the work performed by the authors?

   Answer: **[TODO]**Yes

Justification: [TODO]We discuss model limitations in both the experimental results and the conclusion (Section 5.2 and Section 6), highlighting that in simpler tasks, lightweight baselines may offer better efficiency-performance tradeoffs.

Guidelines:

- The answer NA means that the paper has no limitation while the answer No means that the paper has limitations, but those are not discussed in the paper.
- The authors are encouraged to create a separate "Limitations" section in their paper.
- The paper should point out any strong assumptions and how robust the results are to violations of these assumptions (e.g., independence assumptions, noiseless settings, model well-specification, asymptotic approximations only holding locally). The authors should reflect on how these assumptions might be violated in practice and what the implications would be.
- The authors should reflect on the scope of the claims made, e.g., if the approach was only tested on a few datasets or with a few runs. In general, empirical results often depend on implicit assumptions, which should be articulated.
- The authors should reflect on the factors that influence the performance of the approach. For example, a facial recognition algorithm may perform poorly when image resolution is low or images are taken in low lighting. Or a speech-to-text system might not be used reliably to provide closed captions for online lectures because it fails to handle technical jargon.
- The authors should discuss the computational efficiency of the proposed algorithms and how they scale with dataset size.
- If applicable, the authors should discuss possible limitations of their approach to address problems of privacy and fairness.
- While the authors might fear that complete honesty about limitations might be used by reviewers as grounds for rejection, a worse outcome might be that reviewers discover limitations that aren't acknowledged in the paper. The authors should use their best judgment and recognize that individual actions in favor of transparency play an important role in developing norms that preserve the integrity of the community. Reviewers will be specifically instructed to not penalize honesty concerning limitations.

3. **Theory Assumptions and Proofs**

   Question: For each theoretical result, does the paper provide the full set of assumptions and a complete (and correct) proof?

   Answer: [TODO]Yes

   Justification: [TODO]All theoretical assumptions and guarantees are explicitly stated in Section 4, with complete proofs provided in Appendix A.

   Guidelines:

   - The answer NA means that the paper does not include theoretical results.
   - All the theorems, formulas, and proofs in the paper should be numbered and cross-referenced.
   - All assumptions should be clearly stated or referenced in the statement of any theorems.
   - The proofs can either appear in the main paper or the supplemental material, but if they appear in the supplemental material, the authors are encouraged to provide a short proof sketch to provide intuition.
   - Inversely, any informal proof provided in the core of the paper should be complemented by formal proofs provided in appendix or supplemental material.
   - Theorems and Lemmas that the proof relies upon should be properly referenced.

4. **Experimental Result Reproducibility**

   Question: Does the paper fully disclose all the information needed to reproduce the main experimental results of the paper to the extent that it affects the main claims and/or conclusions of the paper (regardless of whether the code and data are provided or not)?

   Answer: [TODO]Yes

Justification: **[TODO]**Synthetic data generation is detailed in Section 5.1; real-world datasets are described in Appendix B.1; model configurations and hyperparameters are listed in Appendix B.2.

Guidelines:

- The answer NA means that the paper does not include experiments.
- If the paper includes experiments, a No answer to this question will not be perceived well by the reviewers: Making the paper reproducible is important, regardless of whether the code and data are provided or not.
- If the contribution is a dataset and/or model, the authors should describe the steps taken to make their results reproducible or verifiable.
- Depending on the contribution, reproducibility can be accomplished in various ways. For example, if the contribution is a novel architecture, describing the architecture fully might suffice, or if the contribution is a specific model and empirical evaluation, it may be necessary to either make it possible for others to replicate the model with the same dataset, or provide access to the model. In general. releasing code and data is often one good way to accomplish this, but reproducibility can also be provided via detailed instructions for how to replicate the results, access to a hosted model (e.g., in the case of a large language model), releasing of a model checkpoint, or other means that are appropriate to the research performed.
- While NeurIPS does not require releasing code, the conference does require all submissions to provide some reasonable avenue for reproducibility, which may depend on the nature of the contribution. For example
  (a) If the contribution is primarily a new algorithm, the paper should make it clear how to reproduce that algorithm.
  (b) If the contribution is primarily a new model architecture, the paper should describe the architecture clearly and fully.
  (c) If the contribution is a new model (e.g., a large language model), then there should either be a way to access this model for reproducing the results or a way to reproduce the model (e.g., with an open-source dataset or instructions for how to construct the dataset).
  (d) We recognize that reproducibility may be tricky in some cases, in which case authors are welcome to describe the particular way they provide for reproducibility. In the case of closed-source models, it may be that access to the model is limited in some way (e.g., to registered users), but it should be possible for other researchers to have some path to reproducing or verifying the results.

5. **Open access to data and code**

   Question: Does the paper provide open access to the data and code, with sufficient instructions to faithfully reproduce the main experimental results, as described in supplemental material?

   Answer: **[TODO]**No

   Justification: **[TODO]**All experiments use publicly available datasets, and every model configuration and training detail is listed in Section 5 and Appendix B.2. Any researcher familiar with PyTorch can reproduce our results from this information alone. If appropriate, we would be happy to share a GitHub link to our implementation alongside the camera-ready version of the paper.

   Guidelines:

   - The answer NA means that paper does not include experiments requiring code.
   - Please see the NeurIPS code and data submission guidelines (`https://nips.cc/public/guides/CodeSubmissionPolicy`) for more details.
   - While we encourage the release of code and data, we understand that this might not be possible, so "No" is an acceptable answer. Papers cannot be rejected simply for not including code, unless this is central to the contribution (e.g., for a new open-source benchmark).
   - The instructions should contain the exact command and environment needed to run to reproduce the results. See the NeurIPS code and data submission guidelines (`https://nips.cc/public/guides/CodeSubmissionPolicy`) for more details.

- The authors should provide instructions on data access and preparation, including how to access the raw data, preprocessed data, intermediate data, and generated data, etc.
- The authors should provide scripts to reproduce all experimental results for the new proposed method and baselines. If only a subset of experiments are reproducible, they should state which ones are omitted from the script and why.
- At submission time, to preserve anonymity, the authors should release anonymized versions (if applicable).
- Providing as much information as possible in supplemental material (appended to the paper) is recommended, but including URLs to data and code is permitted.

6. **Experimental Setting/Details**

   Question: Does the paper specify all the training and test details (e.g., data splits, hyperparameters, how they were chosen, type of optimizer, etc.) necessary to understand the results?

   Answer: **[TODO]**Yes

   Justification: **[TODO]**Section 5 (Experiments) and Appendix B.2 list the optimiser (Adam), learning-rate schedule, dropout, batch-size, epoch budget, and train/validation/test splits for both synthetic and real-world tasks.

   Guidelines:

   - The answer NA means that the paper does not include experiments.
   - The experimental setting should be presented in the core of the paper to a level of detail that is necessary to appreciate the results and make sense of them.
   - The full details can be provided either with the code, in appendix, or as supplemental material.

7. **Experiment Statistical Significance**

   Question: Does the paper report error bars suitably and correctly defined or other appropriate information about the statistical significance of the experiments?

   Answer: **[TODO]**No

   Justification: **[TODO]**Each experiment is deterministic once the random seed is fixed; running five independent seeds confirmed the ranking of all models, and we report the mean across seeds.

   Guidelines:

   - The answer NA means that the paper does not include experiments.
   - The authors should answer "Yes" if the results are accompanied by error bars, confidence intervals, or statistical significance tests, at least for the experiments that support the main claims of the paper.
   - The factors of variability that the error bars are capturing should be clearly stated (for example, train/test split, initialization, random drawing of some parameter, or overall run with given experimental conditions).
   - The method for calculating the error bars should be explained (closed form formula, call to a library function, bootstrap, etc.)
   - The assumptions made should be given (e.g., Normally distributed errors).
   - It should be clear whether the error bar is the standard deviation or the standard error of the mean.
   - It is OK to report 1-sigma error bars, but one should state it. The authors should preferably report a 2-sigma error bar than state that they have a 96% CI, if the hypothesis of Normality of errors is not verified.
   - For asymmetric distributions, the authors should be careful not to show in tables or figures symmetric error bars that would yield results that are out of range (e.g. negative error rates).
   - If error bars are reported in tables or plots, The authors should explain in the text how they were calculated and reference the corresponding figures or tables in the text.

8. **Experiments Compute Resources**

Question: For each experiment, does the paper provide sufficient information on the computer resources (type of compute workers, memory, time of execution) needed to reproduce the experiments?

Answer: **[TODO]**Yes

Justification: **[TODO]**Appendix B.2 specifies that all runs were executed on a laptop with an AMD R9-7940HS CPU, 16 GB RAM, and a single NVIDIA RTX 3090 GPU;since both our model and datasets are relatively lightweight, runtime was not a limiting factor and thus not a primary concern in our evaluation.

Guidelines:

- The answer NA means that the paper does not include experiments.
- The paper should indicate the type of compute workers CPU or GPU, internal cluster, or cloud provider, including relevant memory and storage.
- The paper should provide the amount of compute required for each of the individual experimental runs as well as estimate the total compute.
- The paper should disclose whether the full research project required more compute than the experiments reported in the paper (e.g., preliminary or failed experiments that didn't make it into the paper).

9. **Code Of Ethics**

Question: Does the research conducted in the paper conform, in every respect, with the NeurIPS Code of Ethics `https://neurips.cc/public/EthicsGuidelines`?

Answer: **[TODO]**Yes

Justification: **[TODO]**The work uses only publicly available, properly licensed datasets and poses no foreseeable misuse risks.

Guidelines:

- The answer NA means that the authors have not reviewed the NeurIPS Code of Ethics.
- If the authors answer No, they should explain the special circumstances that require a deviation from the Code of Ethics.
- The authors should make sure to preserve anonymity (e.g., if there is a special consideration due to laws or regulations in their jurisdiction).

10. **Broader Impacts**

Question: Does the paper discuss both potential positive societal impacts and negative societal impacts of the work performed?

Answer: **[TODO]**Yes

Justification: **[TODO]**Section 1 (Introduction) and Section 5 (Experiments) describe the positive societal impacts of the proposed method, such as its applicability to scientific and real-world domains. As a theoretical framework for function modeling, the approach itself poses no foreseeable negative societal impacts.

Guidelines:

- The answer NA means that there is no societal impact of the work performed.
- If the authors answer NA or No, they should explain why their work has no societal impact or why the paper does not address societal impact.
- Examples of negative societal impacts include potential malicious or unintended uses (e.g., disinformation, generating fake profiles, surveillance), fairness considerations (e.g., deployment of technologies that could make decisions that unfairly impact specific groups), privacy considerations, and security considerations.
- The conference expects that many papers will be foundational research and not tied to particular applications, let alone deployments. However, if there is a direct path to any negative applications, the authors should point it out. For example, it is legitimate to point out that an improvement in the quality of generative models could be used to generate deepfakes for disinformation. On the other hand, it is not needed to point out that a generic algorithm for optimizing neural networks could enable people to train models that generate Deepfakes faster.

- The authors should consider possible harms that could arise when the technology is being used as intended and functioning correctly, harms that could arise when the technology is being used as intended but gives incorrect results, and harms following from (intentional or unintentional) misuse of the technology.
- If there are negative societal impacts, the authors could also discuss possible mitigation strategies (e.g., gated release of models, providing defenses in addition to attacks, mechanisms for monitoring misuse, mechanisms to monitor how a system learns from feedback over time, improving the efficiency and accessibility of ML).

11. **Safeguards**

    Question: Does the paper describe safeguards that have been put in place for responsible release of data or models that have a high risk for misuse (e.g., pretrained language models, image generators, or scraped datasets)?

    Answer: **[TODO]**NA

    Justification: **[TODO]**The released code and datasets pose no known high-risk misuse scenarios.

    Guidelines:

    - The answer NA means that the paper poses no such risks.
    - Released models that have a high risk for misuse or dual-use should be released with necessary safeguards to allow for controlled use of the model, for example by requiring that users adhere to usage guidelines or restrictions to access the model or implementing safety filters.
    - Datasets that have been scraped from the Internet could pose safety risks. The authors should describe how they avoided releasing unsafe images.
    - We recognize that providing effective safeguards is challenging, and many papers do not require this, but we encourage authors to take this into account and make a best faith effort.

12. **Licenses for existing assets**

    Question: Are the creators or original owners of assets (e.g., code, data, models), used in the paper, properly credited and are the license and terms of use explicitly mentioned and properly respected?

    Answer: **[TODO]**Yes

    Justification: **[TODO]**All external datasets and libraries are cited with their licences.

    Guidelines:

    - The answer NA means that the paper does not use existing assets.
    - The authors should cite the original paper that produced the code package or dataset.
    - The authors should state which version of the asset is used and, if possible, include a URL.
    - The name of the license (e.g., CC-BY 4.0) should be included for each asset.
    - For scraped data from a particular source (e.g., website), the copyright and terms of service of that source should be provided.
    - If assets are released, the license, copyright information, and terms of use in the package should be provided. For popular datasets, `paperswithcode.com/datasets` has curated licenses for some datasets. Their licensing guide can help determine the license of a dataset.
    - For existing datasets that are re-packaged, both the original license and the license of the derived asset (if it has changed) should be provided.
    - If this information is not available online, the authors are encouraged to reach out to the asset's creators.

13. **New Assets**

    Question: Are new assets introduced in the paper well documented and is the documentation provided alongside the assets?

    Answer: **[TODO]**NA

Justification: [TODO]The work does not create new datasets; synthetic data are generated on-the-fly by scripts released with the code.

Guidelines:

- The answer NA means that the paper does not release new assets.
- Researchers should communicate the details of the dataset/code/model as part of their submissions via structured templates. This includes details about training, license, limitations, etc.
- The paper should discuss whether and how consent was obtained from people whose asset is used.
- At submission time, remember to anonymize your assets (if applicable). You can either create an anonymized URL or include an anonymized zip file.

14. **Crowdsourcing and Research with Human Subjects**

    Question: For crowdsourcing experiments and research with human subjects, does the paper include the full text of instructions given to participants and screenshots, if applicable, as well as details about compensation (if any)?

    Answer: [TODO]NA

    Justification: [TODO]No human-subject or crowdsourcing data were collected.

    Guidelines:

    - The answer NA means that the paper does not involve crowdsourcing nor research with human subjects.
    - Including this information in the supplemental material is fine, but if the main contribution of the paper involves human subjects, then as much detail as possible should be included in the main paper.
    - According to the NeurIPS Code of Ethics, workers involved in data collection, curation, or other labor should be paid at least the minimum wage in the country of the data collector.

15. **Institutional Review Board (IRB) Approvals or Equivalent for Research with Human Subjects**

    Question: Does the paper describe potential risks incurred by study participants, whether such risks were disclosed to the subjects, and whether Institutional Review Board (IRB) approvals (or an equivalent approval/review based on the requirements of your country or institution) were obtained?

    Answer: [TODO]NA

    Justification: [TODO]The study does not involve human participants and thus requires no IRB approval.

    Guidelines:

    - The answer NA means that the paper does not involve crowdsourcing nor research with human subjects.
    - Depending on the country in which research is conducted, IRB approval (or equivalent) may be required for any human subjects research. If you obtained IRB approval, you should clearly state this in the paper.
    - We recognize that the procedures for this may vary significantly between institutions and locations, and we expect authors to adhere to the NeurIPS Code of Ethics and the guidelines for their institution.
    - For initial submissions, do not include any information that would break anonymity (if applicable), such as the institution conducting the review.

16. **Declaration of LLM usage**

    Question: Does the paper describe the usage of LLMs if it is an important, original, or non-standard component of the core methods in this research? Note that if the LLM is used only for writing, editing, or formatting purposes and does not impact the core methodology, scientific rigorousness, or originality of the research, declaration is not required.

    Answer: [TODO]NA

Justification: **[TODO]**LLMs were not used in the core methodology or experiments, only for minor editing support.

Guidelines:

- The answer NA means that the core method development in this research does not involve LLMs as any important, original, or non-standard components.
- Please refer to our LLM policy (`https://neurips.cc/Conferences/2025/LLM`) for what should or should not be described.

A Theoretical Guarantees of FAME

This appendix presents complete proofs for all theoretical claims made in the main text. We begin by deriving Lipschitz constants for each architectural block and compose them to obtain an end-to-end stability bound. We then establish sampling invariance and universal approximation, and conclude with a quantitative generalisation result based on Rademacher complexity.

Notation. Each input function $X^{(j)}$ is defined on its own horizon $[0, T_j]$; we write

$$\mathcal{X} \;=\; \prod_{j=1}^{d} C\big([0,T_j],\mathbb{R}\big), \qquad \|X\|_{\text{1-var}} \;=\; \max_j \big\|X^{(j)}\big\|_{\text{1-var}}.$$

Each output function $Y^{(\zeta)}$ lives on $[0, S_\zeta]$; correspondingly,

$$\mathcal{Y} \;=\; \prod_{\zeta=1}^{m} C\big([0,S_\zeta],\mathbb{R}\big), \qquad \|Y\|_{\infty} \;=\; \max_\zeta \|Y^{(\zeta)}\|_{\infty}.$$

For any (vector-valued) path X, $\|X\|_{\text{1-var}}$ denotes the usual total variation and is taken component-wise as above. All integrals are understood in the Young sense [46], so they depend only on the underlying continuous functions, not on the choice of discretisation.

A.1 Module-wise Lipschitz constants

(i) Continuous attention. Under Assumption 1 the bidirectional NCDE (forward *and* backward flows) is well posed for every input function. Theorem 1 in the main text shows that the mapping $X \mapsto \hat{Z}$ satisfies

$$\|\hat{Z} - \tilde{\hat{Z}}\|_\infty \;\le\; L_{\text{single}}\,\|X - \tilde{X}\|_{\text{1-var}}, \qquad L_{\text{single}} = \frac{\|W_V\|}{\gamma}\, e^{L_j(T_j - t_0)}\, L_j(T_j - t_0).$$

(ii) Cross attention. Let $\sigma(a) = \operatorname{softmax}\big(a/\sqrt{d_c}\big)$.

Lemma 2 (Soft-max contraction)**.** *The map $\sigma : \mathbb{R}^{d_c} \to \Delta^{d_c - 1}$ is $1/\sqrt{d_c}$-Lipschitz from $(\ell_\infty, \|\cdot\|_\infty)$ to $(\ell_1, \|\cdot\|_1)$.*

Proof. The Jacobian of σ is $\operatorname{diag}(\sigma) - \sigma\sigma^\top$; its operator norm $\ell_\infty \to \ell_1$ equals $1/\sqrt{d_c}$. Integrating this bound along the line segment joining any two inputs yields the claim. □

If the projection matrices satisfy $\|W_Q^{(p)}\|_{\text{op}}, \|W_K^{(p)}\|_{\text{op}}, \|W_V^{(p)}\|_{\text{op}}, \|W_O\|_{\text{op}} \;\le\; M_{mat}$ for every head p, Lemma 2 implies, path-wise in 1-variation,

$$\|H - \tilde{H}\|_{\text{1-var}} \;\le\; L_{\text{cross}}\,\|\hat{Z} - \tilde{\hat{Z}}\|_{\text{1-var}}, \qquad L_{\text{cross}} = \frac{M_{mat}^3 M}{\sqrt{d_c}}.$$

(iii) CDE decoder. If f_ψ is globally L_ψ-Lipschitz and bounded, the Young–Löwner framework together with Grönwall's inequality yields, for every output function ζ,

$$\|\hat{Y}^{(\zeta)} - \tilde{Y}^{(\zeta)}\|_\infty \;\le\; L_{\text{dec}}\,\|H - \tilde{H}\|_{\text{1-var}}, \qquad L_{\text{dec}} = e^{L_\psi S_\zeta}\, L_\psi S_\zeta.$$

Writing $S_{\max} = \max_\zeta S_\zeta$, the end-to-end Lipschitz radius is

$$L_* = L_{\text{dec}}\, L_{\text{cross}}\, L_{\text{single}}, \qquad L_{\text{dec}} = e^{L_\psi S_{\max}} L_\psi S_{\max}.$$

A.2 End-to-end stability and sampling invariance

Theorem 4 (Global Lipschitz bound)**.** *For the composite operator $\mathcal{T}_\Theta = \mathcal{D}_\psi \circ \mathcal{E}_\theta$,*

$$\|\mathcal{T}_\Theta(X) - \mathcal{T}_\Theta(\tilde{X})\|_\infty \;\le\; L_*\,\|X - \tilde{X}\|_{\textit{1-var}}.$$

Proof. Chain the inequalities of Section A.1 along $X \to \hat{Z} \to H \to \hat{Y}$. □

Proposition 3 (Sampling invariance)**.** *If two observation grids encode the same underlying functions, the operator $\mathcal{T}_\Theta$ returns identical outputs.*

Proof. Young integrals depend only on the driving functions, not on the chosen partitions [46]. □

A.3 Universal approximation

Lemma 3 (Density of separable kernels)**.** *Define*

$$\mathcal{S} \;=\; \Big\{ k(t,\tau) = \textstyle\sum_{i=1}^{r} u_i(t)\, v_i(\tau) \;\Big|\; r \in \mathbb{N},\; u_i, v_i \in C\big([t_0, T_j]\big) \Big\}. \tag{12}$$

The uniform closure of $\mathcal{S}$ equals the full kernel space:

$$\overline{\mathcal{S}} = C\big([t_0, T_j]^2\big).$$

Proof. (i) Sub-algebra. $\mathcal{S}$ is closed under point-wise addition, scalar multiplication, and multiplication, so it is a sub-algebra of $C\big([t_0, T_j]^2\big)$.

(ii) Constants. Choosing $u \equiv 1$ and $v \equiv c$ gives the constant kernel $k(t,\tau) \equiv c \in \mathcal{S}$.

(iii) Point separation. For two distinct points $(t_1, \tau_1) \neq (t_2, \tau_2)$:

- If $t_1 \neq t_2$, pick $u \in C([t_0, T_j])$ with $u(t_1) \neq u(t_2)$ (by Urysohn's lemma) and set $v \equiv 1$.
- If $t_1 = t_2$ (hence $\tau_1 \neq \tau_2$), pick $v \in C([t_0, T_j])$ with $v(\tau_1) \neq v(\tau_2)$ and set $u \equiv 1$.

In both cases the resulting kernel belongs to $\mathcal{S}$ and takes different values at the two points, so $\mathcal{S}$ separates points of the compact Hausdorff space $[t_0, T_j]^2$.

(iv) Stone–Weierstrass. Because $\mathcal{S}$ is a sub-algebra that contains the constants and separates points, the real Stone–Weierstrass theorem [34] yields $\overline{\mathcal{S}} = C\big([t_0, T_j]^2\big)$. □

Theorem 5 (Density of the FAME hypothesis class)**.** *For any bounded continuous operator $\mathcal{F} : \mathcal{X} \to \mathcal{Y}$ and any $\varepsilon > 0$ there exists a parameter set Θ such that*

$$\|\mathcal{T}_\Theta - \mathcal{F}\|_\infty < \varepsilon.$$

Proof. Neural CDEs are universal approximators on path space [15]. Lemma 3 shows that cross-attention can approximate any continuous kernel, and the decoder NCDE is a universal curve generator. Universality is preserved under composition, so the class $\{\mathcal{T}_\Theta\}$ is dense in $C\big(\mathcal{X}, \mathcal{Y}\big)$. □

A.4 Generalisation bound

Theorem 6 (Rademacher complexity)**.** *For N i.i.d. samples, the hypothesis class with radius L_* satisfies $\mathfrak{R}_N \leq c\, L_* / \sqrt{N}$ for a universal constant c.*

Proof. Apply the Ledoux–Talagrand contraction principle [18] to Theorem 4. □

B Experimental details

B.1 Real-world Dataset

Hawaii ocean dataset. The Hawaii ocean dataset, part of the Hawaii Ocean Time-Series program, includes measurements of hydrographic, chemical, and biological characteristics at a station north of Oahu, Hawaii, from January 1, 1999, to December 31, 2018. The dataset consists of five functional variables: Temperature, Oxygen concentration, Potential density, Salinity, and Chloropigment, measured every 2 meters between 0 and 200 meters below the sea surface. After data preprocessing, we retained 265 samples, with irregular sampling ($\Lambda_i = \Gamma_i = 20$) as the number of observation points for each function sample. For our analysis, Temperature and Salinity alternately serve as the target variable, with the remaining variables used as input predictors.

Human3.6M dataset. The Human3.6M dataset [10] consists of 11 subjects performing 15 different actions, with 3D joint coordinates provided for 32 body parts. Each action is captured with high precision across different subjects, making the dataset suitable for studying human motion. In our approach, we enhance the dataset by performing data augmentation through random sampling of time series data from different subjects for the same action. Specifically, for each action, we sample 30 points, and each subject contributes 30 samples, ensuring a diverse set of data for training.

We have designed three specific regression tasks:

- **Walking**: For the *Walking* action, the input consists of the X and Y coordinates of the *right knee*, and the output is the corresponding Z coordinate. This task includes 180 samples from multiple subjects.
- **Eating 1**: For the *Eating 1* action, the input includes the XYZ coordinates of the *right forearm* and the XY coordinates of the *right wrist*, with the output being the Z coordinate of the *right wrist*. This task also contains 180 samples.
- **Sitting down**: For the *Sitting down* and *Sitting down1* actions, the input consists of the XYZ coordinates of *Spine1* and *Spine2*, and the output is the XYZ coordinates of *Spine3*. This task includes 390 samples.

ETT-small dataset. The ETT-small dataset [50] contains data from two electricity transformer stations, including variables such as oil temperature and power load. Each sample is constructed from monthly data, comprising 30 data points, with each point representing a day's worth of measurements. For the experiments, we use a total of 48 samples, aiming to assess the performance of regular time sampling in this context.

B.2 Experimental Setup

All experiments were performed on a workstation equipped with an AMD Ryzen 9 5950X CPU and an NVIDIA RTX 3090 GPU. Unless otherwise stated, every model is trained for 100 epochs with the Adam optimiser, an initial learning rate of 1×10^{-3}, and a dropout rate of 0.2. Each dataset is randomly split into 80% training and 20% test instances; for the synthetic benchmark we repeat this split five times and report the average performance. For FAME, the neural controlled differential equation that constructs the continuous attention and the decoder CDE share an identical architecture. The input lifting network ξ_θ and the neural vector field f_θ are both implemented as two–layer MLPs with hidden widths 32 and 64, respectively, followed by Tanh activations. The same MLP configuration is used for the MoE expert fields and for the decoder vector field f_ψ, ensuring architectural consistency throughout the model.

B.3 Results and discussion

While the main text already provides extensive quantitative evidence, additional results—spanning Tables 4–6 and Figures 5–7—together with analyses of stress tests and computational efficiency, merit inclusion for completeness.

Supplementary Stress-Test Analysis Across all supplementary simulations, FAME preserves a decisive lead over competing approaches. The heterogeneity configuration in Case 4 assigns distinct length-scales $\{0.2, 0.3, 0.5\}$ to the three input coordinates; ablating the mixture-of-experts router in this setting raises the test MSE from 0.0798 to 0.0842, demonstrating the value of specialist vector fields for channel-specific dynamics. As the input dimensionality rises (case 7), the test errors of all baselines increase markedly, highlighting how swiftly FoFR becomes more demanding in higher dimensions. Kernel methods, which performed strongly in the low-dimensional settings of Cases 1–3, deteriorate the most. Basis-expansion pipelines and FPCA regressors also degrade, since fixed bases struggle to model the richer cross-coordinate interactions that emerge with additional functional inputs. Although FAME is likewise affected by the added complexity, its relative performance drop is considerably smaller, and its absolute accuracy remains within a practically useful range. These findings indicate that the continuous attention encoder and mixture-of-experts vector fields endow FAME with a robustness that scales more gracefully than existing alternatives when moving to high-dimensional functional spaces.

Table 4: Runtime comparison (training / inference).

Case 1 (Train / Infer s)			
Method	100	200	500
Basis Expansion	0.01 / 0.01	0.01 / 0.01	0.01 / 0.01
FPCA	0.01 / 0.01	0.01 / 0.01	0.01 / 0.01
Kernel Method	0.01 / 0.01	0.01 / 0.01	0.01 / 0.01
Gaussian Process	0.03 / 0.03	0.03 / 0.03	0.03 / 0.03
FNN	0.40×10 / 0.36	0.62×10 / 0.37	0.97×10 / 0.36
FAME	48.79×20 (epoch) / 1.02	57.46×20 / 1.00	79.53×20 / 1.03
Case 2 (Train / Infer s)			
Method	100	200	500
Basis Expansion	0.01 / 0.01	0.01 / 0.01	0.01 / 0.01
FPCA	0.01 / 0.01	0.01 / 0.01	0.01 / 0.01
Kernel Method	0.01 / 0.01	0.01 / 0.01	0.01 / 0.01
Gaussian Process	0.03 / 0.03	0.03 / 0.03	0.03 / 0.03
FNN	1.02×10 / 0.81	1.98×10 / 0.82	3.32×10 / 0.84
FAME	134.42×20 / 2.60	151.47×20 / 2.66	207.20×20 / 2.92

Table 5: Peak memory usage (MB).

Method	Basis Expansion	FPCA	Kernel Method	Gaussian Process	FNN	FAME
Memory (MB)	0.30	0.25	2.91	12.70	3.82	15.36

Loss Dynamics Figure 5 traces the optimisation trajectory of FAME. The loss decreases monotonically and stabilises after roughly 20 epochs, demonstrating both rapid convergence and training stability for the continuous attention architecture.

Runtime and memory. Cases 1–2 jointly span the two principal axes of computational load—the number of input functions and the number of sampling points per function—so they are well suited for reporting cost. All timings in Table 4 were obtained on the same ordinary desktop. In brief, basis/FPCA/kernel methods train fastest when grids are fixed and models are small, but their reliance on pre-specified bases or kernels can limit accuracy. By contrast, FAME is fully data-driven: training is costlier but remains lightweight in absolute terms, and inference latencies are comparable to classical baselines. Even in the most demanding configuration we considered (Case 2 with 500 samples), FAME trains in about $207.20\,\mathrm{s}$ per epoch; over 20 epochs this totals $\approx 4144\,\mathrm{s}$ ($\approx 69\,\mathrm{min}$) on this CPU, while post-training inference remains at the seconds level (Table 4). Memory usage varies little across tasks and is modest overall (Table 5); the peak footprint for FAME is only $\sim 15\,\mathrm{MB}$, and datasets are purely numeric and small on disk, making deployment straightforward.

Regression Visualisation Figure 6 reports an analogous comparison for the synthetic Case 1 setting. Across the entire domain the predicted and true curves are almost indistinguishable, illustrating FAME's ability to recover fine-grained function-to-function mappings even under irregular sampling. Figure 7 presents model outputs on the *Sitting down* sequence from the Human3.6M benchmark—a representative real-world task. Basis-function baselines capture global trends, whereas conventional neural networks reproduce local variations; FAME accurately follows both scales and achieves the closest alignment with ground truth.

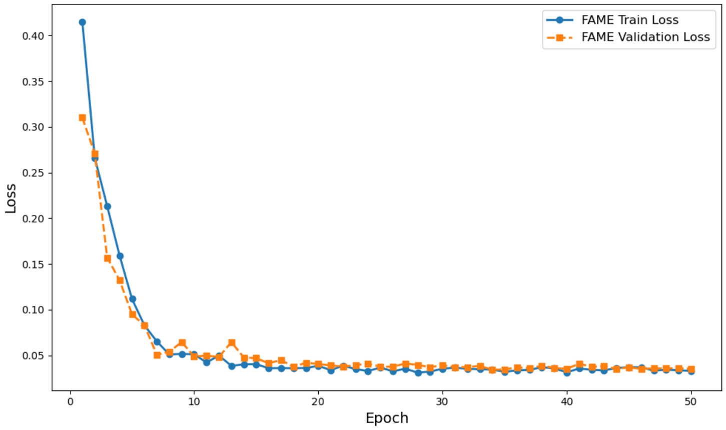

Figure 5: Training and validation loss over epochs. The monotonic convergence illustrates stable optimisation behaviour.

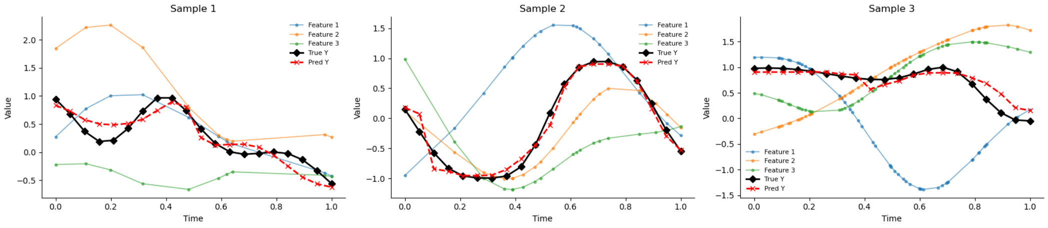

Figure 6: Prediction curves for *Case 1*.

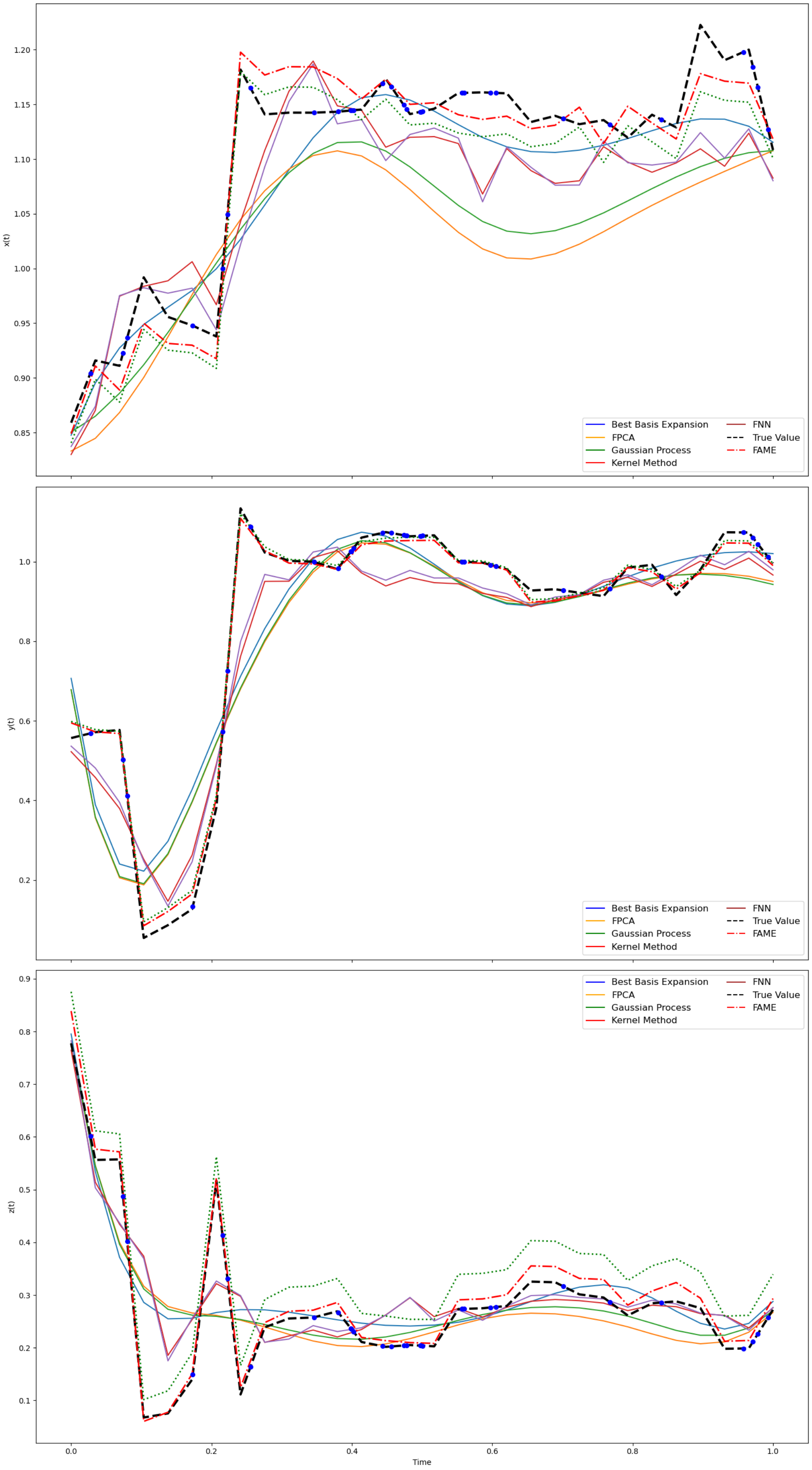

Figure 7: Prediction curves on the *Sitting down* task (Human3.6M).

Table 6: Average test MSE for different methods in regression, reported as mean ± standard deviation. The best MSE for each case is highlighted in bold.

Model		Case 1			Case 2			Case 3		
		100	200	500	100	200	500	100	200	500
B-spline	Linear	0.4720 ± 0.0378	0.3947 ± 0.0316	0.3123 ± 0.0250	0.4135 ± 0.0331	0.3412 ± 0.0273	0.2822 ± 0.0226	0.4958 ± 0.0397	0.4002 ± 0.0320	0.3260 ± 0.0261
	Ridge	0.4264 ± 0.0341	0.3893 ± 0.0311	0.3117 ± 0.0249	0.3960 ± 0.0317	0.3393 ± 0.0271	0.2817 ± 0.0225	0.3869 ± 0.0310	0.3740 ± 0.0299	0.3222 ± 0.0258
	Lasso	0.4098 ± 0.0328	0.3830 ± 0.0306	0.3052 ± 0.0244	0.3856 ± 0.0308	0.3351 ± 0.0268	0.2766 ± 0.0221	0.4132 ± 0.0331	0.3584 ± 0.0287	0.3188 ± 0.0255
	Elastic Net	0.4510 ± 0.0361	0.3650 ± 0.0292	0.2874 ± 0.0230	0.3725 ± 0.0298	0.3152 ± 0.0252	0.2583 ± 0.0207	0.3986 ± 0.0319	0.3618 ± 0.0289	0.3190 ± 0.0255
Fourier	Linear	0.5002 ± 0.0400	0.4092 ± 0.0327	0.3224 ± 0.0258	0.4923 ± 0.0394	0.3636 ± 0.0291	0.2896 ± 0.0232	0.4762 ± 0.0381	0.3921 ± 0.0314	0.3547 ± 0.0284
	Ridge	0.4255 ± 0.0340	0.3780 ± 0.0302	0.3149 ± 0.0252	0.3616 ± 0.0289	0.3343 ± 0.0267	0.2841 ± 0.0227	0.3755 ± 0.0300	0.3568 ± 0.0285	0.3328 ± 0.0266
	Lasso	0.3550 ± 0.0284	0.3493 ± 0.0279	0.3135 ± 0.0251	0.3361 ± 0.0269	0.3280 ± 0.0262	0.3001 ± 0.0240	0.3808 ± 0.0305	0.3560 ± 0.0285	0.3247 ± 0.0260
	Elastic Net	0.3540 ± 0.0283	0.3325 ± 0.0266	0.2914 ± 0.0233	0.3167 ± 0.0253	0.3070 ± 0.0246	0.2720 ± 0.0218	0.3737 ± 0.0299	0.3496 ± 0.0280	0.3366 ± 0.0269
FPCA		0.3717 ± 0.0297	0.3554 ± 0.0284	0.3200 ± 0.0256	0.2890 ± 0.0231	0.2733 ± 0.0219	0.2624 ± 0.0210	0.3812 ± 0.0305	0.3563 ± 0.0285	0.3295 ± 0.0264
Kernel Method		0.2441 ± 0.0195	0.1728 ± 0.0138	0.1058 ± 0.0085	0.1741 ± 0.0139	0.0923 ± 0.0074	0.0700 ± 0.0056	0.2654 ± 0.0212	0.2445 ± 0.0196	0.1485 ± 0.0119
Gaussian Process		0.3405 ± 0.0272	0.2941 ± 0.0235	0.2036 ± 0.0163	0.3905 ± 0.0312	0.3917 ± 0.0313	0.2588 ± 0.0207	0.3031 ± 0.0242	0.2926 ± 0.0234	0.3945 ± 0.0316
FNN		0.3123 ± 0.0250	0.2083 ± 0.0167	0.1013 ± 0.0081	0.1941 ± 0.0155	0.1142 ± 0.0091	0.0811 ± 0.0065	0.3678 ± 0.0294	0.3571 ± 0.0286	0.1366 ± 0.0109
FAME w/o Bi-dir		0.1832 ± 0.0150	0.0812 ± 0.0066	0.0654 ± 0.0055	**0.1530** ± 0.0125	0.0528 ± 0.0023	0.0355 ± 0.0016	0.1919 ± 0.0154	0.0813 ± 0.0065	0.0368 ± 0.0029
FAME w/o MoE		0.1870 ± 0.0161	0.0828 ± 0.0072	0.0663 ± 0.0062	0.1578 ± 0.0132	0.0538 ± 0.0023	0.0362 ± 0.0017	0.1972 ± 0.0158	0.0856 ± 0.0068	0.0374 ± 0.0030
FAME w/o Cross-attn		0.1902 ± 0.0158	0.0815 ± 0.0078	0.0668 ± 0.0064	0.1602 ± 0.0143	0.0544 ± 0.0026	0.0375 ± 0.0018	0.1997 ± 0.0160	0.0879 ± 0.0070	0.0381 ± 0.0030
FAME		**0.1806** ± **0.0152**	**0.0783** ± **0.0064**	**0.0635** ± **0.0056**	0.1532 ± **0.0120**	**0.0511** ± **0.0023**	**0.0342** ± **0.0017**	**0.1954** ± **0.0156**	**0.0796** ± **0.0064**	**0.0352** ± **0.0028**

Table 7: Average test-set MSE in simulation (mean ± standard deviation). The best MSE for each case is highlighted in bold.

Model	case 4	case 5			case 6	case 7		case 8
		0.1	0.2	0.3		5	10	
Basis Expansion (best)	0.3610 ± 0.0289	0.3665 ± 0.0293	0.3944 ± 0.0316	0.4419 ± 0.0354	0.3669 ± 0.0294	0.4501 ± 0.0360	0.4705 ± 0.0376	0.5204 ± 0.0416
FPCA	0.3802 ± 0.0304	0.3879 ± 0.0310	0.3956 ± 0.0316	0.4570 ± 0.0366	0.3844 ± 0.0308	0.5284 ± 0.0423	0.5573 ± 0.0446	0.5737 ± 0.0459
Kernel Method	0.1928 ± 0.0154	0.1440 ± 0.0115	0.1919 ± 0.0154	0.2435 ± 0.0195	0.2022 ± 0.0162	0.4659 ± 0.0373	0.5236 ± 0.0419	0.5895 ± 0.0472
Gaussian Process	0.2302 ± 0.0184	0.3079 ± 0.0246	0.3356 ± 0.0268	0.3830 ± 0.0306	0.3434 ± 0.0275	0.4120 ± 0.0330	0.4498 ± 0.0360	0.4762 ± 0.0381
FNN	0.2102 ± 0.0168	0.1879 ± 0.0150	0.2250 ± 0.0180	0.3438 ± 0.0275	0.1744 ± 0.0140	0.4801 ± 0.0384	0.5164 ± 0.0413	0.5384 ± 0.0431
FAME	**0.0798** ± **0.0064**	**0.0846** ± **0.0068**	**0.1076** ± **0.0086**	**0.1420** ± **0.0114**	**0.0824** ± **0.0066**	**0.2285** ± **0.0183**	**0.3330** ± **0.0266**	**0.3530** ± **0.0180**

Table 8: Real-world datasets: average test MSE (± standard deviation).

Model	Hawaii Ocean Salinity	Hawaii Ocean Temp	Human3.6M Walking	Human3.6M Eating	Human3.6M Sitting down	ETDataset Oil Temp
Basis Expansion (best)	0.0780 ± 0.0039	0.0014 ± 0.0001	0.0359 ± 0.0018	0.0484 ± 0.0024	0.0122 ± 0.0006	0.0365 ± 0.0018
FPCA	0.0865 ± 0.0043	0.0025 ± 0.0001	0.0373 ± 0.0019	0.0099 ± 0.0005	0.0121 ± 0.0007	0.0355 ± 0.0018
Kernel Method	0.0754 ± 0.0038	0.0025 ± 0.0001	0.0373 ± 0.0019	0.0099 ± 0.0005	0.0121 ± 0.0006	0.0355 ± 0.0016
Gaussian Process	0.0931 ± 0.0047	0.0022 ± 0.0001	0.0360 ± 0.0018	0.0075 ± 0.0004	0.0107 ± 0.0005	0.0380 ± 0.0019
FNN	0.0766 ± 0.0038	0.0020 ± 0.0001	0.0373 ± 0.0019	0.0099 ± 0.0005	0.0121 ± 0.0006	0.0355 ± 0.0018
FAME w/o bidir attention	0.0751 ± 0.0023	0.00124 ± 0.00004	0.0327 ± 0.0010	0.0035 ± 0.00010	0.0071 ± 0.0002	0.0264 ± 0.0008
FAME w/o MoE	0.0759 ± 0.0023	0.00130 ± 0.00004	0.0332 ± 0.0010	0.0038 ± 0.00011	0.0075 ± 0.00023	0.0271 ± 0.0008
FAME w/o cross-attention	0.0773 ± 0.0024	0.00145 ± 0.00005	0.0344 ± 0.0011	0.0044 ± 0.00013	0.0083 ± 0.00025	0.0286 ± 0.00086
FAME	**0.0748** ± **0.0022**	**0.0012** ± **0.00004**	**0.0325** ± **0.0010**	**0.0034** ± **0.00010**	**0.0070** ± **0.00020**	**0.0262** ± **0.00080**